Bioprinting 43 (2024) e00359

Contents lists available at ScienceDirect

Bioprinting

journal homepage: www.sciencedirect.com/journal/bioprinting

Precision 3D printing of chitosan-bioactive glass inks: Rheological optimization for enhanced shape fidelity in tissue engineering scaffolds

Larissa R. Lourenço [a], Roger Borges [b], Danilo Carastan [c], Mônica B. Mathor [d], Juliana Marchi [a,*]

[a] Centro de Ciências Humanas e Naturais (CCNH), Universidade Ferderal do ABC (UFABC), Brazil
[b] School of Biomedical Engineering, Faculdade Israelita de Ciências da Saúde Albert Einstein, Hospital Israelita Albert Einstein, Brazil
[c] Centro de Engenharia, Modelagem e Ciências Sociais Aplicadas (CECS), Universidade Ferderal do ABC (UFABC), Brazil
[d] Centro de Tecnologia das Radiações (CETER), Instituto de Pesquisas Energéticas e Nucleares (IPEN), Brazil

ARTICLE INFO

Keywords:
Chitosan
Bioactive glass
3D printing
Processability
Tissue engineering

ABSTRACT

3D printing technology in tissue engineering applications provides several advantages for scaffold development, especially with natural materials, such as chitosan, which provides a biomimetic environment for cellular growth. However, chitosan hydrogel-based inks still show poor printing fidelity. In this article, we overcame this challenge by incorporating bioactive glasses (BG) nanoparticles (up to 5 wt%) into the chitosan hydrogel. The resulting inks were characterized by rheological tests, while their processability was evaluated through measurements of shape fidelity. An indirect cytotoxicity assay was also conducted to evaluate the cell viability of the printed scaffolds. The results indicated that adding BG nanoparticles to the chitosan-based ink modified its rheological properties and improved its shape-fidelity during 3D printing, which we suggest are consequences of hydrogen bonds established between the glass and the chitosan chains. Also, cytotoxicity assessment demonstrated that the resulting scaffold exhibits high cell viability. In conclusion, the proposed composite ink has optimized rheological properties for 3D printing and is promising for applications in tissue engineering.

1. Introduction

Traditional polymer processing techniques for producing three-dimensional scaffolds include but are not limited to casting, electrospinning, phase separation, and lyophilization. Despite their widespread use in scaffold production, they have certain disadvantages that limit their use in tissue engineering. These disadvantages include their lack of reproducibility, limited control over porosity, challenges in constructing structures large 3D pieces, and complex design [1]. In contrast, 3D printing has been gaining prominence in various applications due to its ability to overcome many of these limitations, being an excellent alternative in various applications.

Additive manufacturing, or 3D printing, encompasses techniques developed since the late 1980s, and over the last decade, it has been increasingly applied in tissue engineering [2]. The main advantages of 3D printing include achieving high reproducibility and control over the structural properties of materials, such as porosity and surface area, which are essential characteristics for tissue growth, angiogenesis, and nutrient transport. Furthermore, 3D printing also allows designs that closely resemble the complexity of the body's architecture, enabling biomimetic strategies to assist in the regenerative process. Additionally, imaging technologies such as computed tomography and magnetic resonance allow the modeling of structures of interest for constructing patient-specific scaffolds based on personalized medicine strategies [3].

Microextrusion 3D printing allows the use of hydrogels, which are viscoelastic materials able to absorb a significant amount of water, thus providing fluid absorption, nutrient exchange, and a suitable environment for cell development [4]. Because they are able to mimic the properties of various tissues, hydrogels have been widely used in tissue engineering [5]. However, an overcoming challenge in extrusion-based 3D printing is the optimization of the hydrogel rheological properties, as rheology influences the printing process and shape fidelity of the resulting printed scaffold [6–8].

Among the 3D printed materials applied in tissue engineering, chitosan is an attractive alternative due to its biocompatibility and cost-effectiveness. Chitosan is a linear copolymer obtained by partial deacetylation of chitin, composed of β-(1 → 4) D-glucosamine and β-(1 → 4) N-acetyl-D-glucosamine monomers. The amino group (-NH_2) in chitosan's structure allows it to dissolve in acidic solutions (pH < 6.5) and, when protonated, provides a cationic character to the polymer,

* Corresponding author.
E-mail address: juliana.marchi@ufabc.edu.br (J. Marchi).

https://doi.org/10.1016/j.bprint.2024.e00359
Received 19 June 2024; Received in revised form 10 September 2024; Accepted 16 September 2024
Available online 18 September 2024

enabling interactions with lipids, DNA, and negatively charged polymers [9].

Chitosan can form two types of hydrogels (i) chemical, characterized by predominantly covalent bonds formed through the addition of substances (such as glutaraldehyde, glycidyl ether, diisocyanate, and genipin) that mediate the formation of covalent crosslinks within the polymeric network; (ii) physical, characterized by secondary bonds, including hydrophobic interactions (induced by changes in pH or acetylation [10,11]), hydrogen bonds (intermolecular or with the solvent) and electrostatic interactions (crosslinking mediated by ions or negatively charged molecules like citrates [12]). While chemical hydrogels offer greater control over their physical-chemical properties and better mechanical performance, the crosslink additives often contain toxic materials, which can hinder or even preclude their use in biomedical applications. Therefore, physical hydrogels are more suitable in this field [13].

Combined with bioactive glasses (BG) as a composite, chitosan-based hydrogels display enhanced regenerative capacity for hard and soft tissues. Bioactive glasses were developed in 1971 by L. Hench, and since then, their primary application has been in the regeneration of bone and dental tissues [14]. Their success in regenerating mineralized tissues is attributed to their bioactivity, which is their ability to form strong bonds with the bone by forming a hydroxyapatite layer on its surface after ion exchange reactions with the body fluid [15]. Furthermore, releasing constituent ions, such as calcium, phosphate, and silicon species, can promote cell proliferation, differentiation, and more general processes like angiogenesis and anti-inflammatory effects [16]. Besides, adding bioactive glass to a polymeric matrix can increase wettability, improve cell adhesion, and act as a mechanical reinforcement filler for the composite [17]. Composites based on chitosan and bioactive glass have been explored since the early 2000s [18,19], with their primary applications focused on bone tissue, periodontal applications, wound dressings, and drug delivery. Such composite combines chitosan's biomimetic properties for cell growth with cellular signaling through ion release and bioactivity provided by the bioactive glass [20]. However, the potential of this material in various areas that already use chitosan and bioactive glass separately, such as in cartilaginous tissue and, more recently, nervous tissue, has not yet been explored.

Polymer/bioactive glass composites have been produced by additive manufacturing, employing robocasting [21] and other 3D printing techniques [22,23]. Most of the available literature has evaluated the effect of bioactive glass particles on polymeric hydrogels, like gelatin-alginate-hyaluronic acid [22], polycaprolactone-chitosan [24], and alginate-methyl cellulose-trimethyl chitosan [23]. However, to the best of the authors' knowledge, the evaluation of bioactive glass in chitosan ink in terms of its suitability for 3D printing has not yet been reported. Therefore, this study aims to develop chitosan ink with different concentrations of bioactive glass, then assess their rheological properties and evaluate shape fidelity and *in vitro* cytotoxicity of the printed structures.

2. Materials and methods

2.1. 58S bioactive glass synthesis and characterization

The synthesis of the 58S bioactive glass (58 % SiO_2-33 % CaO-9% P_2O_5, in wt%) was performed by the quick alkali sol-gel method developed by Xia and Chang [25] and adapted by our research group [26]. Tetraethyl orthosilicate (TEOS, Sigma Aldrich, 98 %) and triethyl phosphate (TEP, Sigma Aldrich, 98 %) were hydrolyzed in an acidic solution containing distilled water, ethanol (Sigma Aldrich, 99.5 %), and nitric acid (2M, Merck, 65 %). After 20 min of stirring calcium nitrate tetrahydrate (Sigma Aldrich, 99.997 %) was added to the mixture, and the new solution was stirred again for 20 min. Subsequently, ammonium hydroxide (2M, Casa Americana, MW 35.05 g/mol) was added, resulting in the gelation of the colloidal solution. The solution was freeze-dryed (Operon, South Korea) for 24 h, and the powder was calcined at 550 °C/1h with a heating rate of 10 °C/min (Furnace 300, EDG, Brazil). The powder glass (BG) was milled and sieved (40 μm) before producing the printing inks. Finally, the glass powder was incubated for 72 h in Dulbecco Modified Eagle's DMEM at 37 °C. Subsequently, it was washed (distilled water, 3x) and dried at 50 °C for 24 h. This last step was employed to reduce the initial cytotoxicity of bioactive glasses when tested in 2D static cell culture. The 58S bioactive glass powder was characterized through scanning electron microscopy (JSM-6010LA, Jeol, Japan) and ATR-FTIR (attenuated total reflectance Fourier-transform infrared spectroscopy, Spectrum Two FT-IR, PerkinElmer, United States) in the range between 1400 and 500 cm^{-1}, 64 scans per sample. The results are presented in supporting information (SP1). Other characterizations of the BG used in this work can be found elsewhere [27,28].

Table 1
Composition of the inks used in this work.

Composition	Chitosan concentration [w/v %]	BG concentration [w/v%]	Mass proportion BG:Quitosana
C6	6	–	–
CBG0.5	6	0.5	0.08:1
CBG1	6	1	0.17:1
CBG2	6	2	0.33:1
CBG5	6	5	0.83:1

2.2. Preparation and rheological characterization of the composite inks

Chitosan hydrogels were prepared according to the protocol presented by Wu et al. [29]. Initially, we prepared a solution containing 40 % acetic acid, 10 % lactic acid, and 3 w/v% citric acid in distilled water. Subsequently, 6 w/v% of chitosan (low molecular weight, degree of deacylation ≥85 %, Sigma Aldrich) and bioactive glass nanoparticles at different concentrations, described in Table 1, were added into the acid solution, for now on named as C6, CBG0.5, CBG1, CBG2, and CBG5, respectively. After 12 h, the mixtures were homogenized in ultrasound (Q1.8, Ecosonic, Brazil) for 2 h and centrifuged (Excelsa II, FANEM, Brazil) at 3600 rpm for 30 min.

The inks were rheologically characterized through oscillatory and continuous measurements performed at room temperature in a modular compact rheometer (MCR-502, Anton Paar, Austria). A cone-plate geometry (25 mm diameter and 1° angle) and parallel plate geometry (25 mm diameter and 0.5 mm gap) were used for oscillatory and rotational experiments, respectively.

The linear viscoelastic region (LVR) of the materials was estimated by the amplitude sweep test, applying an angular frequency of 1 rad/s. The storage (G') and loss (G") moduli were measured as a function of oscillatory amplitude in the 0.1 - 100 % range. The frequency sweep was performed within the LVR, with a deformation amplitude of 1 %. The material moduli were measured as a function of angular frequency in the 0.1 - 300 rad/s range.

The flow curve tests were conducted in triplicate, and the material's viscosity as a function of shear rate in the range of 0.1 - 15 s^{-1} was measured. A regression analysis of the curves was performed using Origin 8.5 software to obtain the rheological parameters of the materials. A modified model of the Carreau-Yasuda curve was applied, representing materials that exhibit a viscosity plateau at high shear rates, followed by a decrease in the viscosity value according to the Power Law, as expressed by eq (1) [30].

$$\eta(\dot{\gamma}) = \frac{\eta_0}{\left[1 + (\lambda\dot{\gamma})^a\right]^{\left(\frac{1-n}{a}\right)}} \times 100 \quad (1)$$

Where η_0 is the viscosity when the shear rate is zero, η is the viscosity of

the material, $\dot{\gamma}$ is the shear rate, λ is a time constant equal to the inverse of the shear rate at the transition from constant viscosity to variable viscosity, "a" is a parameter defining the curvature of the plateau-to-decline transition, and "n" is the exponent of the Power Law, which determines the slope coefficient of the viscosity variation curve [29]. It is essential to highlight that in the Carreau-Yasuda Equation, higher values of "n" imply a less inclined slope of the curve.

The recovery tests were conducted in triplicate, and the viscosity of the materials was measured using the Three-Interval Thixotropy Test (3ITT) model with the following parameters: i) shear rate of 0.1 s^{-1} applied for 60 s; ii) shear rate of 10 s^{-1} applied for 30 s; iii) the shear rate was returned to 0.1 s^{-1} for 120 s. This experimental procedure aims to simulate the events that occur during 3D printing by extrusion, making it possible to evaluate the percentage of material recovery after shearing, which is calculated by considering the ratio of the material's viscosity values before and after the shearing event. The recovery percentage indicates the ability of the inks to recover to their original structure.

2.3. Evaluation of materials processability, scaffold production, and characterization

The chitosan-based inks were printed using an Octopus™ microextruder (3D Biotechnology Solutions, Brazil), a 19 G (0.7 mm) needle, and a printing speed of 1 mm/s. Computer-aided design (CAD) model construction and the printing file (gcode) generation were carried out using the Tinkercad™ and Slic3r™ software, respectively. After printing, the scaffolds were dried at 50 °C for 24 h (Didática SP, Brazil), neutralized with a 0.5 M sodium hydroxide solution (Casa Americana, MW 40 g/mol) for 2 h at a ratio of 10 mL/cm^2. The scaffolds were washed three times with distilled water. The neutralization step is essential to guarantee that the scaffold pH is adequate for use in the human body. Additionally, the physical chitosan hydrogel produced has elements that act as ionic crosslinkers (citrates), and a pH close to neutrality reduces the protonation and repulsion of chitosan-free amino groups, favoring the crosslinking and stability of the hydrogel.

The shear rate during the printing process ($\dot{\gamma}$) was estimated to compare the rheological data with the printing process. Such parameters can be obtained with correction relative to the variation of velocity distribution occurring in non-Newtonian materials (Equation (2), where n = viscoelasticity index [6]). The volumetric flow rate (Q) was calculated using Equation (3), where A is the printed area, and v is the flow rate [31], which was adjusted by the CAD software itself (Slic3r) [32]. The area was determined by approximating the printed filament to the shape of a cylinder with the same radius as the extrusion needle (r = 0.35 mm). The height of the cylinder, denoted as "h," was considered 1 mm, given that the printing speed was 1 mm/s. When these values are substituted into Equation (3), the result is Q = 0.27 mm^3/s.

$$\dot{\gamma} = \frac{4Q}{\pi r^3} \times \frac{3n+1}{4n} \tag{2}$$

$$Q = Av = \pi r^2 hv = 0,27\ mm^3/s \tag{3}$$

The ink processability was assessed by printing (in triplicate) in a grid pattern in a single layer. Photographs of the printed structures were then analyzed using ImageJ software. Two parameters were chosen to evaluate the shape fidelity of the materials: the pore area of the grid structure and the filament thickness. These parameters were calculated by comparing the printed model with the theoretical data from the CAD model, as shown in Equations (4) and (5) [7]. The filament thickness (W) was evaluated by comparing the thickness of the printed filaments with the diameter of the printing needle, a method developed by Kang et al. [33]. The ideal value of W is equal to 1, indicating no difference between the thickness of the printed filament and the needle diameter, as shown in Equation (5).

$$Shape\ Fidelity\ (\%) = \frac{\text{Pore area of the printed structure}}{\text{Pore area of CAD model}} \tag{4}$$

$$W = \frac{Mean\ filament\ width}{Needle\ diameter} \tag{5}$$

The structure of the printed scaffolds was evaluated by scanning electron microscopy (JSM-6010LA, Jeol, Japan), operating in secondary electron detection mode, with an electron beam of 11-15 kV. The scaffolds were fixed on aluminum stubs coated with conductive carbon tape. The *in vitro* degradation assay was carried out to evaluate the weight loss percentage of the materials with the addition of BG. The scaffolds were incubated in PBS at 37 °C for 28 days. At specific periods (1, 2, 3, 7, 14, 21, and 28 days), the scaffolds were dried and their weight was measured. The weight loss percentage (WL%) was estimated using Equation (6), where W_f is the final weight of the scaffold and W_i is the initial weight of the scaffold.

$$WL\% = \frac{W_i - W_f}{W_i} \times 100 \tag{6}$$

2.4. Biological characterization of the printed scaffolds

2.4.1. Cell culture

For this assay, the scaffolds on each side were exposed to UV light for 15 min. All manipulations were performed within the laminar flow cabinet. The cell line used in the assay was Balb/c 3T3, a murine embryonic fibroblast cell line (ATCC CCL-163), recommended for *in vitro* cytotoxicity assessment. The cell lines grew adhered in polypropylene containers containing DMEM culture medium supplemented with 10 % fetal bovine serum, 4 mM glutamine, and an antibiotic/antimycotic solution consisting of 100 IU/mL penicillin, 100 μg/mL streptomycin, and 0.025 μg/mL amphotericin B, referred to as D10. The cells were maintained at 37 °C in a CO_2 incubator with 5 % CO_2. Passages were performed following the characteristics of the cell line.

2.4.2. Biological assays by MTS

The indirect cytotoxicity assay was conducted following the ISO 10933-5 guidelines. Extract preparation was carried out over 72 h. A cell density 10^4 was selected, and a 96-well plate was used (n = 5, three independent assays). After a 24-h incubation of the cells in contact with the materials extracts, 100 μL of a solution containing MTS (3-(4,5-dimethylthiazol-2-yl)-5-(3-carboxymethoxyphenyl)-2-(4-sulfophenyl)-2H-tetrazolium), PMS (phenazine methosulfate), and D10, (19/1/80 % v/v ratio, respectively), were added in the wells.

$$Cell\ viability\ \% = \frac{mean\ absorbance\ of\ extracts}{mean\ absorbance\ of\ control} \times 100 \tag{6}$$

For the adhesion assay, the scaffolds were incubated in DMEM for 30 min, cut with a 6 mm punch, and placed in the bottom of the well of a 96-well plate. Then 150 μL of cell suspension containing 2x10^4 cells was added to each well containing the scaffolds, using empty ones for control (n = 5). After incubation for 20h, the cell culture medium was removed and the scaffolds were moved to a previously empty well, to separate the cells adhered to the scaffolds. Then, 150 μL of the same die solution previously used was added to assess cell viability. After incubation for 4h, the absorbance was measured and adhesion was estimated according to Equation (7), where C corresponds to the absorbance of the control group and NA to the absorbance of the cells that did not adhered to the scaffold.

$$Cell\ adhesion\ \% = 100 - \left(\frac{NA}{C} \times 100\right) \tag{7}$$

2.4.3. Proliferation assay

The proliferation assay was conducted by fluorescence microscopy

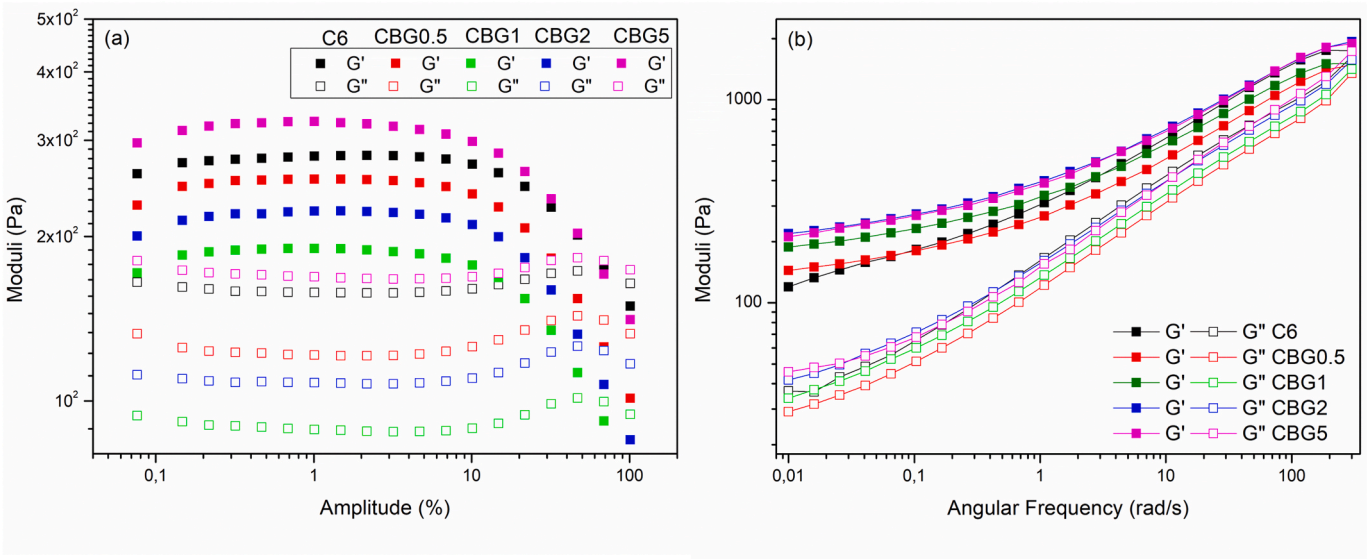

(c)

Material	G' (Pa)	G"(Pa)	Tanδ
C6	119.78	36.77	0.29 ± 0.02
CBG0.5	144.38	29.05	0.21 ± 0.02
CBG1	188.45	33.88	0.20 ± 0.03
CBG2	219.05	41.69	0.20 ± 0.03
CBG5	211.71	45.71	0.24 ± 0.04

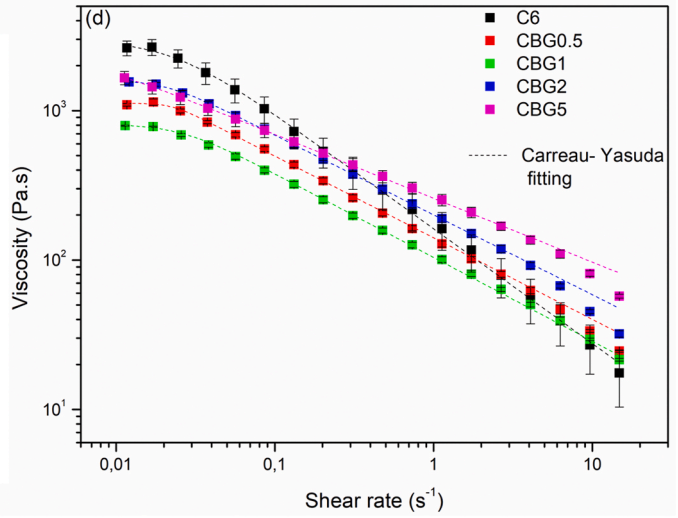

Fig. 1. Behavior of the storage (G′) and loss (G″) moduli obtained during the rheological assays of (a) amplitude and (b) angular frequency; (c) Table of values of G′, G″, and tanδ obtained from the frequency sweep at ω = 0.01 rad/s; (d) Viscosity as a function of shear rate and Carreau-Yasuda fitting for the samples studied in this work.

(INCell Analyzer HS 2500, Cytiva, USA), using the same methodology described for the adhesion assay. After the scaffolds were on the plate, 150 μL of cell suspension containing $5x10^3$ cells was added to each scaffold, and the plate was incubated for 4h for cell adhesion. Then, 15 μL of calcein-AM (1 mM, Sigma Aldrich) was added to each well and the plate was incubated overnight. The micrographs were obtained on days 1, 2, and 3 to quantify the cell growth. Images were analyzed using ImageJ software. For cell count three random areas (200x200 pixels) of different scaffolds (n = 3) were used. The percentage was estimated by comparing the mean values of the second and third days to the initial first-day count. CBG2 and CBG5 samples showed lack of transparency, blocking the fluorescence reading.

2.5. Statistical analysis

A one-way analysis of variance (ANOVA) was employed to assess the significance of the experimental values for the recovery (n = 3) and cytotoxicity (n = 5) assays, followed by the Tukey test. The significance level was set at 5 % (p-valor >0.05). All calculations were conducted using Origin 8.5 software.

3. Results

In this study, five compositions of chitosan ink containing bioactive glass (0, 0.5, 1, 2, and 5 wt%) were produced to evaluate the influence of the BG on the rheological properties and processability of the chitosan-based inks for 3D printing, aiming the development of scaffolds with controlled pore size and complex geometry.

The results of the amplitude sweep (Fig. 1a) show that the linear viscoelastic region (LVR) of the inks lies within the deformation amplitudes range of 0.1 %–10 % for all studied inks. Thus, subsequent experiments were conducted using an amplitude of 1 %, a value within the LVR, employing the SAOS (small amplitude oscillatory shear) method [22]. The results of the storage (G′) and loss (G″) moduli as a function of angular frequency are presented in Fig. 1b. One can note that the elastic behavior is predominant in the inks (G'> G"). However, the modulus values are frequency-dependent within the analyzed range; besides, with the increase in angular frequency, the values of the moduli converge, indicating a tendency to invert the predominant behavior in higher frequencies.

The rheological values in the semi-static condition (0.01 rad/s) of the frequency sweep are shown in Fig. 1c. Higher concentrations of bioactive glass (BG) in chitosan inks lead to higher G' values, which indicates

Table 2
Rheological parameters relative to the Carreau-Yasuda model. η0 is the viscosity when the shear rate is zero, λ is a time constant, "a" is a parameter for the transition from the plateau to the descent line, "n" is the exponent of the Power Law, and R^2 is the regression coefficient.

Ink	η_0 [Pa.s]	λ [s]	n	a	R^2
C6	2972.10 ± 87.27	64.48 ± 3.27	0.230 ± 0.010	2.00[a]	0.997
CBG0.5	1165.65 ± 14.57	25.08 ± 0.69	0.446 ± 0.009	4.32 ± 0.81	0.999
CBG1	813.02 ± 16.50	20.74 ± 1.20	0.440 ± 0.007	2.76 ± 0.65	0.999
CBG2	1600.12 ± 22.05	32.70 ± 0.75	0.466 ± 0.007	3.39 ± 0.47	0.996
CBG5	2240.38 ± 41.87	14.43 ± 0.53	0.572 ± 0.004	2.00[a]	0.999

[a] For these samples, it was not possible to calculate "a" using the software. Therefore, its value was fixed to the one previously proposed by Carreau before the modifications made by Yasuda.

an increase in the elastic behavior of the inks. When observing the G" values (Fig. 1c), there is an initial decrease from C6 to CBG0.5. However, as the BG concentration in the ink increases, there is a subsequent increase in the loss modulus values, with CBG2 surpassing C6. Thus, adding BG particles into chitosan inks modifies the rheological behavior of the ink, affecting the viscoelastic components by different mechanisms and an understanding of such behavior can help us optimize the 3D printing process for such materials, which shall be discussed in the next section.

The G″ and G′ ratio (tanδ, Fig. 1c) is considered an essential parameter in 3D printing, especially for the micro-extrusion process [7]. The tanδ values for the produced inks range from 0.198 (CBG1) to 0.295 (C6), tending to decrease with the increasing concentration of bioactive glass in the chitosan matrix. The relation between tanδ and the material's shape fidelity will be discussed in the next section.

Fig. 1d shows the ink viscosity as a function of the shear rate obtained in the flow curve test, along with the Carreau-Yasuda fitting for the curves. The rheological parameters of the inks are presented in Table 2. The studied chitosan-based inks show a pseudoplastic behavior, with a decrease in viscosity as a function of an increase in shear rate. Furthermore, analyzing the viscosity values in the lower shear rates (<0.1), the presence of bioactive glass in the ink reduces its viscosity. Such behavior does not depend directly on the concentration of BG particles, as viscosity decreases for lower BG concentrations (samples CBG0.5 and CBG1) but is followed by an increase for higher BG concentrations (samples CBG2 and CBG5). Nevertheless, the initial viscosity of all composite materials does not exceed the value of pure chitosan ink, as shown in Fig. 1d and Table 2, considering the calculated values of η_0 (i.e., viscosity at rest).

From the rheological analysis, it was observed that the increase in BG concentration reduces the viscosity's dependency on the shear rate. Such behavior is characterized by "n," the coefficient of the Power Law (see eq (1)), and higher values of "n" imply a less inclined slope, indicating a more stable ink that can maintain its structure while shearing.

After understanding the behavior of the produced inks by applying different shear rates, their viscosity recovery response was studied by simulating the 3D printing process. The results of viscosity over time and the material recovery values are presented in Fig. 2a and b, respectively. In general, recovery higher than 80 % is desired [8]. It was observed that pure ink (C6) has a lower recovery (54.9 %) compared to the ones containing bioactive glass. Furthermore, more significant amounts of glass in the chitosan matrix led to higher recovery, up to 83.2 % (for CBG5). These results corroborate those obtained in the amplitude and shear rate sweep analysis, where bioactive glass in the hydrogel resulted in more gel stability.

The rheological properties of the ink affect the 3D printing process. Thus, the increased stability and recovery behavior of the chitosan ink containing BG particles is essential to expand their use as printing ink. Thus, the 3D printing process shall be explored, considering processability analysis, as well as the structural and biological behavior of the printed scaffolds aimed at tissue engineering applications.

3.1. Processability analysis

Considering the excellent rheological characteristics of the chitosan-containing bioactive glass gels for 3D printing applications, the next step of this work was to use such gels to print the scaffolds through a micro-extrusion 3D printing process. After optimizing printing parameters, that is, 22G needle (0.7 mm) and extrusion velocity of 1 mm/s, the shear rate during printing was calculated using eq (3). The experimental results are presented in the supporting information (SP2). The shear rate of chitosan containing BG is about 9.4-10.5 s^{-1}. Thus, it can be expected that the real recovery percentage for the materials during printing will be very similar to those obtained in the rheological analyses using $\dot{\gamma} = 10\ s^{-1}$ (Table 2).

All materials formed continuous filaments under the printing conditions used in this work. Fig. 3a shows the theoretical CAD model and the printed structures with chitosan-based inks containing BG. By comparing the theoretical model with the structures obtained after 3D printing, it was possible to evaluate the shape fidelity by evaluating the

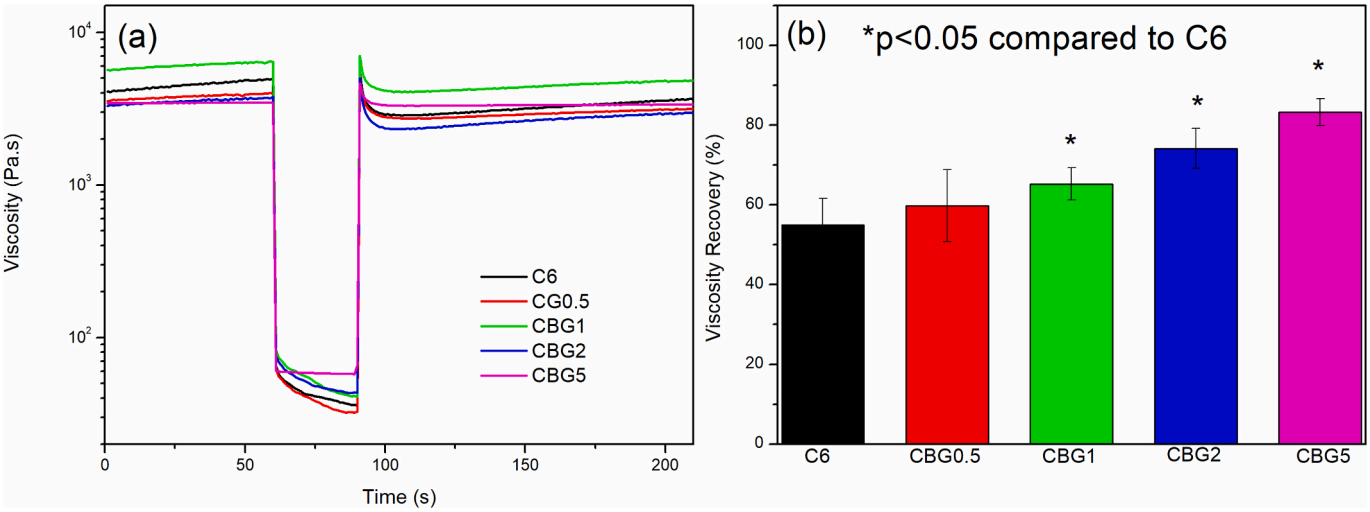

Fig. 2. Rheological results obtained through the recovery assay ($\dot{\gamma} = 10\ s^{-1}$): (a) viscosity over time and (b) the percentage of viscosity recovery of the materials.

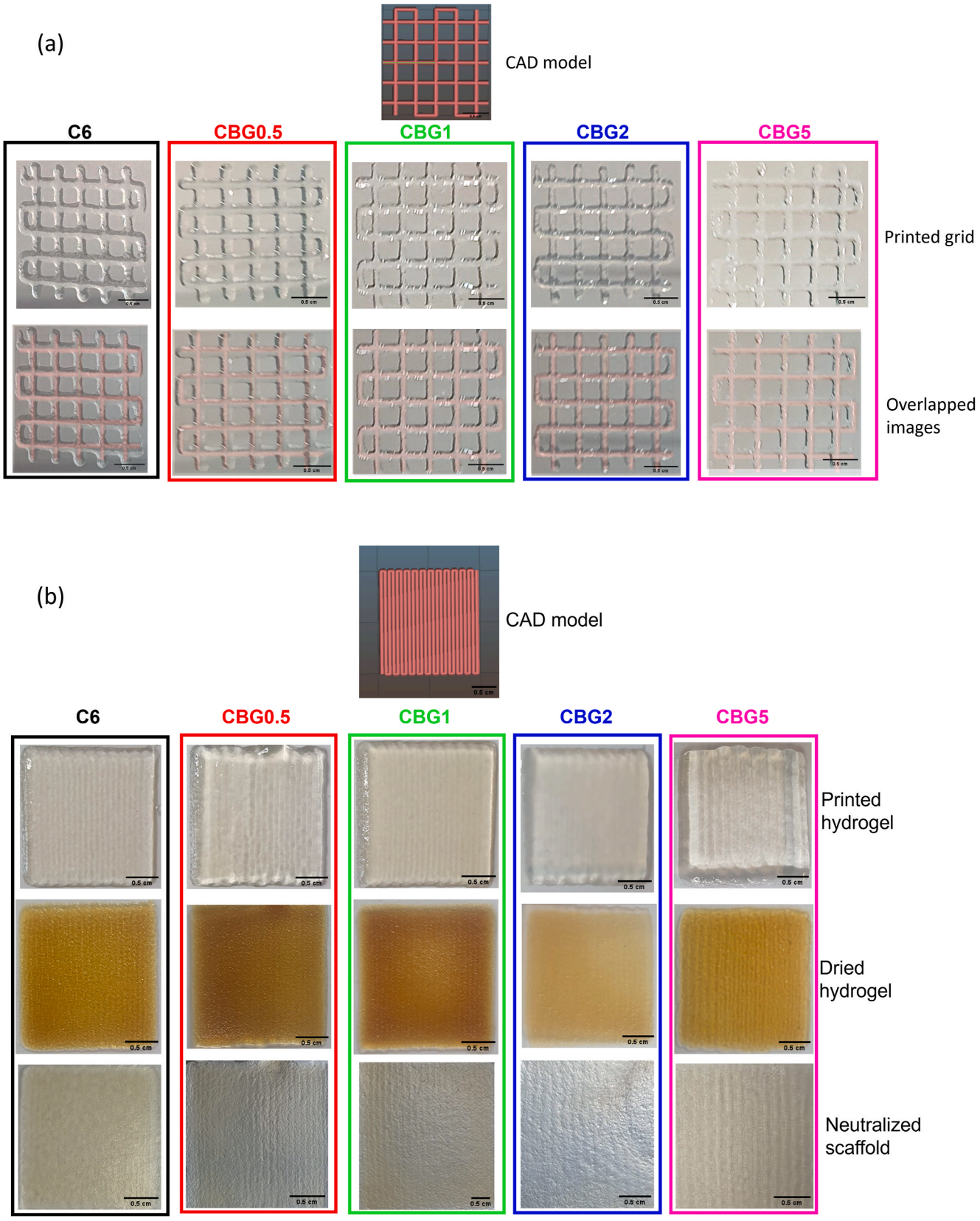

Fig. 3. Representative photographs of the (a) CAD grid model used printed structures and image overlays for qualitative verification of shape fidelity; (b) constructed CAD model, printed hydrogel, scaffold after drying, and the finished scaffold after the neutralization process. Scale bar = 0.5 cm on all images.

Table 3
Comparison between shape fidelity and rheological properties of the studied materials.

Material	Rheological Properties			Shape Fidelity	
	Viscosity at rest, η_0, [Pa.s]	Recovery $10s^{-1}$ [%]	Tanδ	Pore area [%]	Filament width (W)
C6	2972.10 ± 87.27	54.92 ± 11.60	0.29 ± 0.02	62.15 ± 7.27	1.92 ± 0.08
CBG0.5	1165.65 ± 14.57	59.78 ± 9.00	0.21 ± 0.02	70.42 ± 6.94	1.88 ± 0.03
CBG1	813.02 ± 16.50	65.21 ± 5.51	0.20 ± 0.03	90.82 ± 4.61	1.25 ± 0.03
CBG2	1600.12 ± 22.05	74.16 ± 7.88	0.20 ± 0.03	91.78 ± 12.77	1.38 ± 0.02
CBG5	2240.38 ± 41.87	83.21 ± 3.37	0.24 ± 0.04	86.45 ± 6.20	1.37 ± 0.03

pore area and filament thickness (W), which relates to the ratio of filament width to needle diameter. The results are presented in Table 3.

When analyzing W, a decrease in this value with adding bioactive glass to the ink was observed, bringing it closer to its ideal value of W = 1. It implies higher processing accuracy with increased BG concentration, with W values of 1.92, 1.88, and 1.25 for C6, CBG0.5, and CBG1, respectively. However, for the higher glass concentrations (CBG2 and CBG5), the value of W tends to increase (1.38 and 1.37) compared to the other BG-containing inks. Nonetheless, such materials are closer to the ideal W value than C6 and CBG0.5.

In terms of the pore area, it can be observed that there is an increase in such values with BG amount, achieving values greater than 90 %. Samples CBG1 and CBG2 reached 90.8 % and 91.8 %, respectively. After 90 % fidelity, there is a tendency for the stability of this property, as it means higher viscosity and recovery percentage of the inks [7,34]. These results indicate that adding bioactive glass to chitosan hydrogel improved its performance as a 3D printing ink, enhancing both the parameters evaluated for shape fidelity.

3.2. Scaffold characterization

After printing, the scaffolds were dried and neutralized. Fig. 3b shows the CAD model and representative photographs of the hydrogels after the printing and scaffolds after the drying and neutralization process. The material changes can be observed in the post-printing stages. After the drying step, an expected shrinkage of the scaffolds occurs, which is reversed after the rehydration of the materials. However, the surface pattern remains visible at all stages of material processing.

Fig. 4 illustrates the scanning electron microscopy (SEM) images depicting the surfaces and cross-sections of the 3D-printed scaffolds. Concerning the surface morphology (see left column), the C6 scaffold exhibits a notably smoother surface than scaffolds containing bioactive glass. Incorporating bioactive glass into the scaffold composition increases the particles present, consequently enhancing surface roughness. The analysis of the cross-sectional micrographs (right column) reveals a consistently dense, layered structure across all scaffold compositions, with small pores presence. Notably, one can observe that compositions containing bioactive glass display discernible and well-dispersed glass particles within the internal structure of the scaffolds.

The weight loss of the materials during time was studied through the *in vitro* degradation assay, presented in Fig. 5a. The degradation of the C6 sample was the highest, with some samples disintegrated by 14 days of the experiment. Interestingly, the BG addition to the chitosan matrix reduced the degradation degree of the scaffolds: after 28 days the weight loss of the CBG0.5, CBG1, CBG2, and CBG5 were 66.9, 39.0, 30.1, and 11.9 %, respectively. CBG1 was statistically different from CBG5, indicating a dose-dependent behavior.

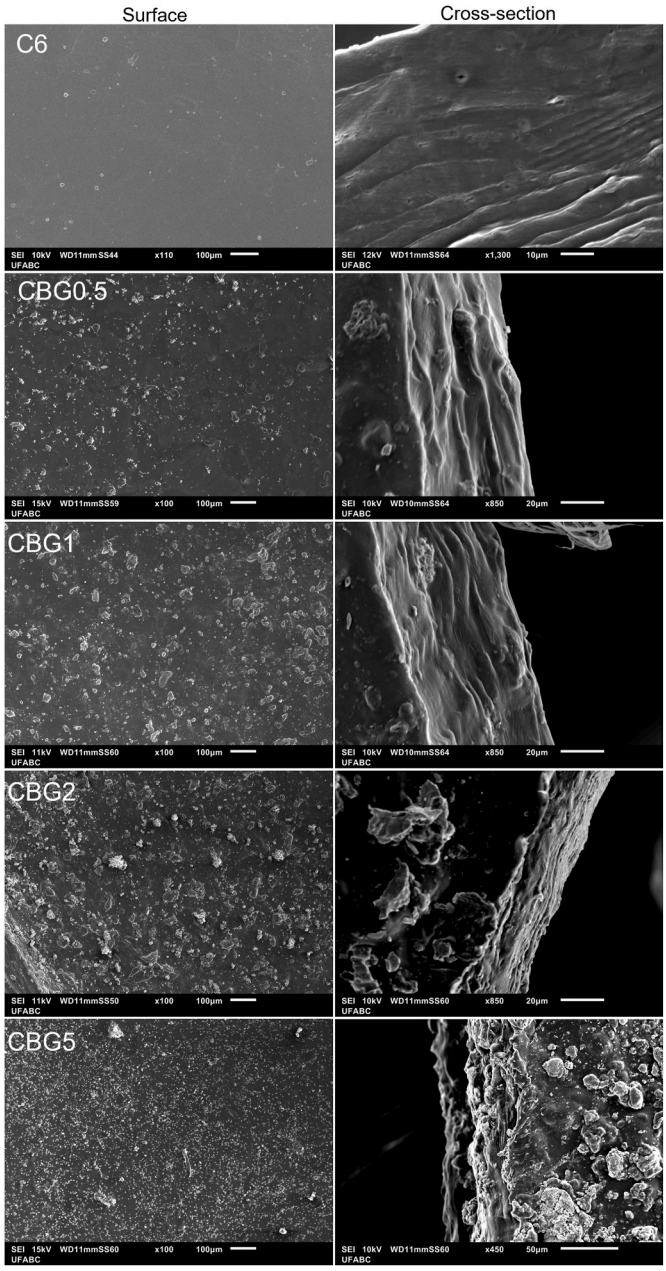

Fig. 4. SEM micrographs of the surface (left column) and cross-section (right column) of the 3D-printed scaffolds. Please note that the scale of the cross-section images of the C6 and CBG5 scaffolds differ from the other compositions, being respectively 10 μm and 50 μm.

3.3. Biological evaluation

Biological characterization was performed on the neutralized scaffolds, using *in vitro* indirect cytotoxicity tests by MTS with fibroblastic cells (Balb/c 3T3) to assess the material's toxicity in tissue engineering applications. Fig. 5b presents the results of the percentage of cell viability for the scaffolds. The graphs are displayed in box plots, illustrating the distribution of results in quartiles, marking the maximum and minimum values obtained, the first quartile, the median, and the third quartile of the data groups, along with the mean values obtained.

All the materials tested have a mean cell viability above 90 %, characterizing the developed scaffolds as non-cytotoxic for this cell type. When evaluating the results obtained in this work, it is noted that C6, CBG0.5, CBG1, and CBG2 achieved viability values with a median above 100 %. Furthermore, a reduction in viability is noticed in conjunction

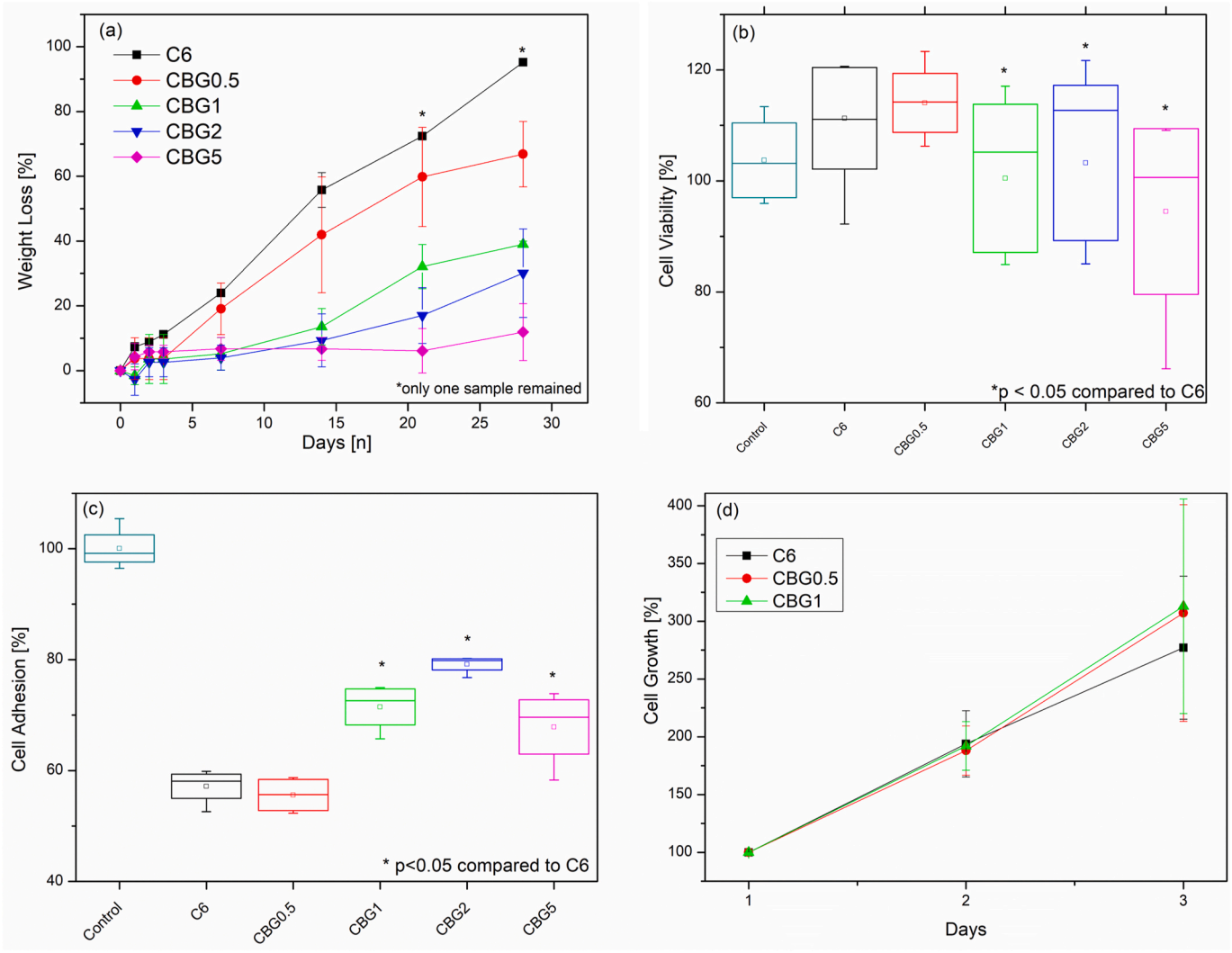

Fig. 5. (a) *In vitro* degradation of the scaffolds on PBS up to 28 days; (b-d): balb/c 3T3 cell experiments: (b) viability; (c) adhesion of balb/c 3T3 cell obtained from the MTS indirect cytotoxicity and adhesion assay, and (d) proliferation behavior obtained from fluorescence microscopy cell count.

with bioactive glass in the chitosan matrix, with statistical differences observed starting from 1 % of glass in the scaffold (CBG1).

Fig. 5c shows the results of the adhesion assay using MTS. Higher BG amounts on the scaffolds increase cell adhesion, from ~52 % to 80 % for CBG2. The scaffold with the highest amount of BG (CBG5) showed a decreased cell adhesion (~68 %).

The cell proliferation on the scaffolds was evaluated using fluorescence microscopy (Fig. 6), with a respective cell growth curve (Fig. 5d). Samples containing the higher glass concentration (CBG2 and CBG5) present absence of transparency that prevents fluorescence analysis. All scaffold compositions allowed adhesion and growth of fibroblastic cells. The data indicated no significant increase in proliferation with the addition of bioactive glass, even though a slight increase was observed on the third day of the assay, with the mean values 277 %, 307 %, and 313 % for C6, CBG0.5, and CBG1 scaffolds, respectively. Additionally, considering the magnification of the micrographs (Fig. 6, left column), the healthy adhered morphology of the cells on the scaffold can be observed, supporting the adhesion assay results.

4. Discussion

The developed inks were analyzed considering their rheological behavior, focusing on the effect of the bioactive glass on the chitosan matrix, and a specific evaluation was performed to envision the application of the materials in 3D printing. The viscoelastic behavior presented by the inks (Fig. 1b), in which the moduli values are dependent on the angular frequency, is characteristic of weak gels. The physical chitosan hydrogel has not yet been crosslinked at this production stage, remaining at an acidic pH. Consequently, there is greater chain repulsion and fewer ionic crosslinks due to the protonation of the amine present in chitosan, resulting in a less stable material and weak gel behavior [12]. Similar properties were observed by Hamdine et al. [35] in chitosan hydrogels produced from organic acids. Such property is desirable since it may favor the material's extrusion and use in 3D printing [36].

Moreover, the rheological characterization of the inks revealed the different effects of the BG particles on the chitosan matrix. Considering the loss modulus (G") of the materials, higher values were measured with the increasing concentration of BG in the ink matrix. This behavior may be attributed to the release of Ca^{2+} by the glass particles since this ion does not act as a cross-linker in the chitosan structure, as demonstrated by Nie et al. [37]. Therefore, the presence of Ca^{2+} in the ink can interfere with the interaction between polymeric chains due to electrostatic interactions between positive charges (Fig. 7a). Furthermore, Yamaguchi et al. [38] studied the influence of different acids in the chitosan/hydroxyapatite nanocomposite formation. The authors reported the formation of COO^{-}-Ca bonds between calcium ions and acids with more than one hydroxyl group in their structure, such as citric acid.

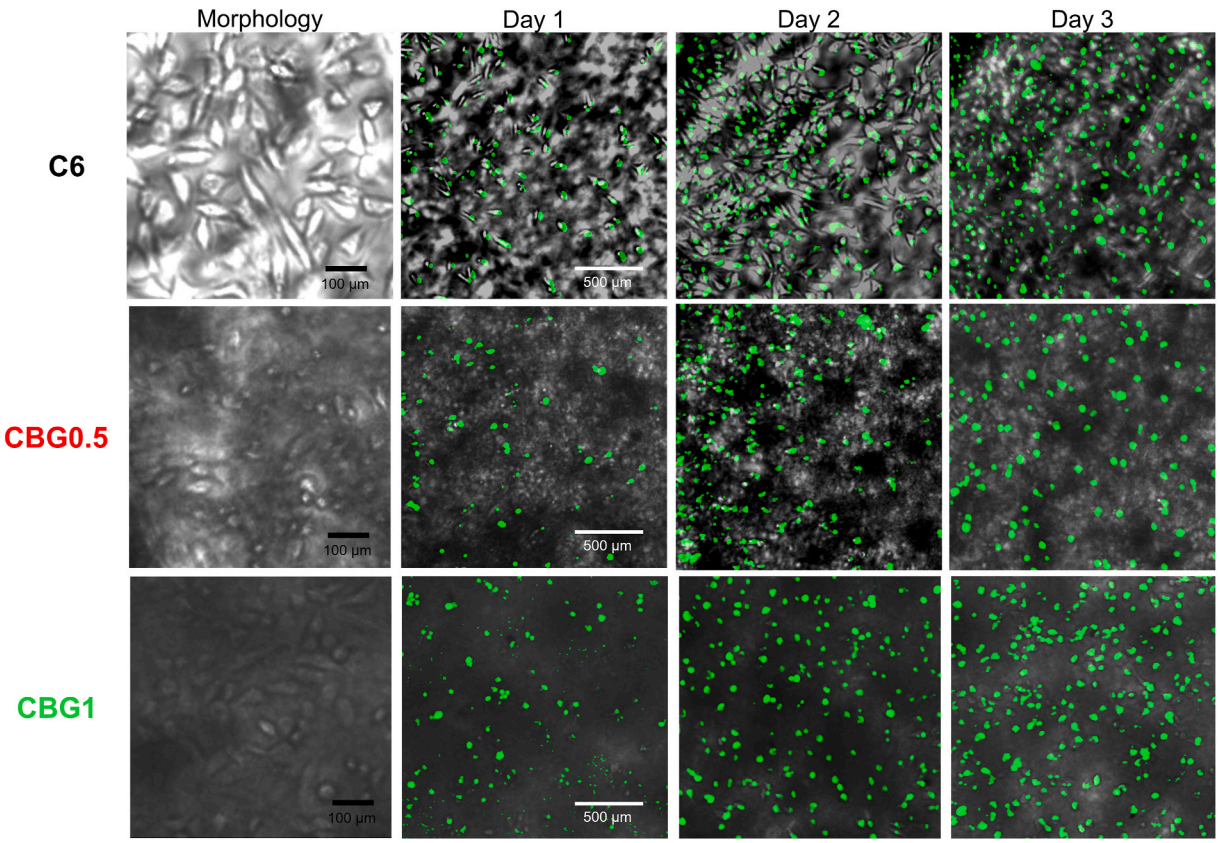

Fig. 6. Fluorescence microscopy of C6, CBG0.5, CBG1 scaffolds with casein marked Balb/c 3T3. The left column is an area under low magnification to observe cell morphology. The subsequent columns display cell amount on different days.

Thus, the calcium ions can hinder the formation of ionic crosslinks between the chitosan chains mediated by citric acid.

When analyzing the storage modulus (G′, Fig. 1b), higher values are observed when bioactive glass is added to the chitosan-based ink. Such behavior was expected once BG is a purely elastic phase incorporated into the hydrogel matrix. Furthermore, studies have shown that hydrogen bonds are formed between the hydroxyl groups on the glass surface and the amines and hydroxyl groups in the chitosan molecule (Fig. 7b) [20,39]. Such an event would enhance the stability of the hydrogel and limit chain movement, affecting the rheological properties of the composite materials [20]. Changes related to this event are an increase in the values of G′, a reduction in the dependence of the materials' viscosity on the shear rate, and higher values of the recovery percentage of the inks. An increase in recovery with bioactive glass addition was also observed for inks composed of methacrylate collagen and bioactive glass [40]. The authors related the presence of bioactive glass to the limited entanglement of polymer chains and an increase in the ionic character of the ink.

The viscosity of the inks displayed an interesting behavior with the addition of the bioactive glass (Fig. 1d), initially reducing (CBG0.5 and CBG1 when compared to C6) and a following increase observed in the two last compositions (CBG2 and CBG5). That is possibly a result of the different mechanisms through which the BG affects the chitosan ink. The initial reduction may result from the Ca^{2+} liberation and interaction with the matrix. At the same time, the subsequent increase could be a consequence of the higher influence of the elastic characteristics displayed by the BG particles.

The rheological properties discussed earlier were summarized in Table 3 to compare the rheological properties and processability of the inks. Possible relations can be made between the rheological results and shape fidelity parameters of the studied inks. There was a tendency for improved shape fidelity with (i) an increase in the ink resting viscosity, (ii) an increase in the ink recovery percentage, and (iii) a reduction in the value of tanδ. Materials with higher viscosities can better maintain their shape after printing [7]. Furthermore, higher recovery indicates a return to the ink's initial structural conditions, which indicates the transition between fluid flow behavior and elastic shape maintenance, potentially helping maintain the material's shape fidelity [34,41].

Regarding the comparison of rheological properties and expected shape fidelity, Gao et al. observed an improvement of this property with an increase in tanδ when evaluating this parameter in a gelatin and alginate hydrogel [42]. It is the opposite behavior of the results observed in this study, where the shape fidelity increased with the decrease of tanδ. Therefore, it highlighted the importance of assessing different rheological properties of materials used in 3D printing and that these properties can indicate different events depending on the material under evaluation.

The characterization of the scaffold allows the evaluation of the materials ' properties for tissue engineering. The reduction of scaffold degradation with BG addition is possibly a consequence of the increased stability of the material containing BG (Fig. 5a), which could reduce chain movement and liquid uptake [43]. This dependence is a very interesting property, once the degradation period to a specific tissue and application can be optimized. Aiming bone tissue regeneration, Guo et al. [20] observed similar behavior of chitosan containing BG scaffolds.

Along with improving the inks' processability and shape fidelity, the BG's presence in the inks also presented interesting biological results (Fig. 5b). It was observed that all compositions but CBG5 had cell viability higher than 100 %, which indicates that the ink extract may have a proliferative character or increase cell metabolic activity, favoring the metabolization of the dying substance. These results follow those obtained by Wu et al., who achieved high cell viability chitosan scaffolds through an indirect cytotoxicity assay using Alamar blue and L929 fibroblast cell lines [29]. The increase in cell viability can be

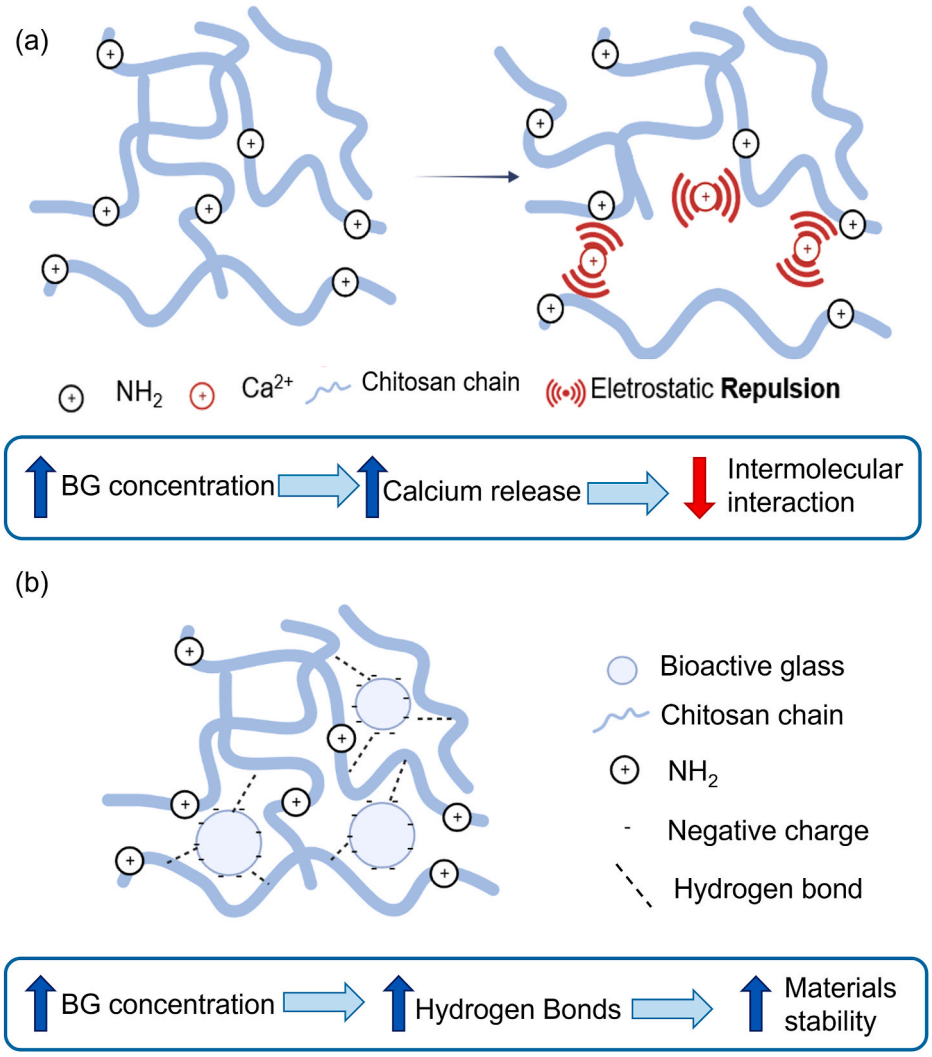

Fig. 7. Simplified representations of (a) the interaction of Ca^{2+} with the polymeric matrix, and (b) hydrogen bond formation between chitosan molecules and BG particles. Created with BioRender

exciting in tissue engineering and indicates that this material should be further studied and applied in the field.

Another observation regarding the cytotoxicity assay was the decrease of viability in the materials with higher concentrations of BG. This effect of bioactive glass dissolution *in vitro* tests is known in the literature. It is caused by the ions released by the bioactive glass, which affect the pH of the culture medium and can be detrimental to cells [44]. However, it is already understood that the body's homeostatic mechanisms prevent harmful effects from occurring *in vivo*, and no toxic responses have been observed in the kidneys and liver due to the degradation of the bioactive glass [45]. Therefore, although a reduction in cell viability caused by bioactive glass in the matrix was identified, the developed scaffolds can be characterized as non-toxic based on releasing their elements and degradation residues, making them suitable for potential use in tissue regeneration.

BG addition improved cell adhesion to the scaffold (Fig. 5c). Additionally, the cells displayed an adhered morphology (Fig. 6). Such behavior could be related to the distinct morphological properties exhibited by the different scaffold compositions. In this context, it is known that increased surface roughness, the presence of particles, and porosity can enhance the biomimetic nature of the surface and facilitate cell adhesion [46]. That is because biological tissues have complex arrangements at the nanoscale in their basal membrane, and interaction between cells and a surface with complex topography becomes more natural [47]. The proliferation evaluation (Figs. 5d and 6) showed that the constructed structures supported cell growth and development. Considering adhesion and proliferation as crucial factors that mediate the regenerative processes, the overall results showed that the produced scaffolds have promising properties for tissue engineering applications.

5. Conclusion

Chitosan-bioactive glass composites have been explored in various areas of tissue engineering. This work aimed to enhance their application by producing materials with optimized characteristics for 3D printing. The rheological characterization of the developed inks revealed that bioactive glass addition affects their rheological properties through two concurrent factors: the presence of glass particles (hydrogen bonds) and the release of calcium ions in the ink. Furthermore, the increased ink stability resulting from the hydrogen bonds between chitosan and the glass surface improved material recovery, reaching values greater than 80 %. The effect of the changes in the rheological properties of the materials was observed in the subsequent evaluation of the processability of the inks. Adding bioactive glass to the chitosan matrix increased the accuracy and shape fidelity of the printed structures, meaning it enhanced the material's performance as a 3D printing ink, with shape fidelity exceeding 90 %. The concentration of BG can also be used to control the degradation degree of the scaffolds.

Regarding *in vitro* biological properties, the scaffolds are non-cytotoxic to fibroblastic and show high cell viability. Moreover, the presence of bioactive glass increased cell adhesion to the scaffolds, and all materials support cell development. Therefore, the produced composites show promise for use in 3D printing and can potentially enhance applications in tissue engineering.

Data and code availability

The experimental data is available under demand.

Ethical approval

Not Applicable.

CRediT authorship contribution statement

Larissa R. Lourenço: Writing – original draft, Investigation, Formal analysis, Data curation. **Roger Borges:** Writing – original draft, Investigation, Formal analysis. **Danilo Carastan:** Writing – review & editing, Visualization, Validation, Methodology. **Mônica B. Mathor:** Writing – review & editing, Visualization, Validation, Methodology, Conceptualization. **Juliana Marchi:** Writing – review & editing, Writing – original draft, Visualization, Validation, Supervision, Resources, Project administration, Methodology, Conceptualization.

Declaration of competing interest

The authors declare that they have no known competing financial interests or personal relationships that could have appeared to influence the work reported in this paper.

Data availability

Data will be made available on request.

Acknowledgments

The authors thank the financial support from FAPESP (Fundação de Amparo a Pesquisa do Estado de São Paulo, 2020/00329-6), CNPq (Conselho Nacional de Desenvolvimento Científico e Tecnológico, 311280/2023-4) and Capes (Coordenação de Aperfeiçoamento de Pessoal de Nível Superior, cod 001). CEM-UFABC and laboratory infrastructure from UFABC and IPEN/CETER are appreciated. We would also like to acknowledge the experimental support of MSc. Matheus Mendes, MSc. Vanessa Magalhães, Fernanda Barna, and Giovanna Dias. The proliferation assays experiments were conducted in Incell equipament, under the expertise of Dr. Daniel Perez Vieira (IPEN/CETER), who is also acknowledged.

Appendix A. Supplementary data

Supplementary data to this article can be found online at https://doi.org/10.1016/j.bprint.2024.e00359.

References

[1] L.R. Yadav, S.V. Chandran, K. Lavanya, N. Selvamurugan, Chitosan-based 3D-printed scaffolds for bone tissue engineering, Int. J. Biol. Macromol. 183 (2021) 1925–1938, https://doi.org/10.1016/j.ijbiomac.2021.05.215.
[2] A. Zaszczyńska, M. Moczulska-Heljak, A. Gradys, P. Sajkiewicz, Advances in 3D printing for tissue engineering, Materials 14 (2021) 3149, https://doi.org/10.3390/ma14123149.
[3] M. Sahranavard, A. Zamanian, F. Ghorbani, M.H. Shahrezaee, A critical review on three dimensional-printed chitosan hydrogels for development of tissue engineering, BioPrint. 17 (2020) e00063, https://doi.org/10.1016/j.bprint.2019.e00063.
[4] D.J. Beebe, J.S. Moore, J.M. Bauer, et al., Functional hydrogel structures for autonomous flow control inside microfluidic channels, Nature 404 (2000) 588–590, https://doi.org/10.1038/35007047.
[5] S. Mantha, S. Pillai, P. Khayambashi, et al., Smart hydrogels in tissue engineering and regenerative medicine, Materials 12 (2019) 3323, https://doi.org/10.3390/ma12203323.
[6] M. Rahimnejad, T. Labonté-Dupuis, N.R. Demarquette, S. Lerouge, A rheological approach to assess the printability of thermosensitive chitosan-based biomaterial inks, Biomed. Mater. 16 (2021) 015003, https://doi.org/10.1088/1748-605X/abb2d8.
[7] S. Bom, R. Ribeiro, H.M. Ribeiro, et al., On the progress of hydrogel-based 3D printing: correlating rheological properties with printing behaviour, Int. J. Pharm. 615 (2022) 121506, https://doi.org/10.1016/j.ijpharm.2022.121506.
[8] P.A. Amorim, M.A. d'Ávila, R. Anand, et al., Insights on shear rheology of inks for extrusion-based 3D bioprinting, BioPrint. 22 (2021) e00129, https://doi.org/10.1016/j.bprint.2021.e00129.
[9] J. Ahmed, M. Mulla, M. Maniruzzaman, Rheological and dielectric behavior of 3D-printable chitosan/graphene oxide hydrogels, ACS Biomater. Sci. Eng. 6 (2020) 88–99, https://doi.org/10.1021/acsbiomaterials.9b00201.
[10] A. Montembault, C. Viton, A. Domard, Rheometric study of the gelation of chitosan in aqueous solution without cross-linking agent, Biomacromolecules 6 (2005) 653–662, https://doi.org/10.1021/bm049593m.
[11] S. Ladet, L. David, A. Domard, Multi-membrane hydrogels, Nature 452 (2008) 76–79, https://doi.org/10.1038/nature06619.
[12] J. Berger, M. Reist, J.M. Mayer, et al., Structure and interactions in covalently and ionically crosslinked chitosan hydrogels for biomedical applications, Eur. J. Pharm. Biopharm. 57 (2004) 19–34, https://doi.org/10.1016/S0939-6411(03)00161-9.
[13] P. Sacco, F. Furlani, G. De Marzo, et al., Concepts for developing physical gels of chitosan and of chitosan derivatives, Gels 4 (2018) 67, https://doi.org/10.3390/gels4030067.
[14] A.R. Boccaccini, D.S. Brauer, L. Hupa, Bioactive Glasses: Fundamentals, Technology and Applications, Royal Society of Chemistry, Cambridge, 2016.
[15] J.R. Jones, Review of bioactive glass: from Hench to hybrids, Acta Biomater. 9 (2013) 4457–4486, https://doi.org/10.1016/j.actbio.2012.08.023.
[16] V. Miguez-Pacheco, L.L. Hench, A.R. Boccaccini, Bioactive glasses beyond bone and teeth: emerging applications in contact with soft tissues, Acta Biomater. 13 (2015) 1–15, https://doi.org/10.1016/j.actbio.2014.11.004.
[17] S. Kargozar, R.K. Singh, H.-W. Kim, F. Baino, "Hard" ceramics for "Soft" tissue engineering: paradox or opportunity? Acta Biomater. 115 (2020) 1–28, https://doi.org/10.1016/j.actbio.2020.08.014.
[18] El-Bassyouni GT, Mohamed K Characterization and In-Vitro Behavior of Bioactive Glass/Polymeric Composites.
[19] A.j. Asikainen, J. Hagström, T. Sorsa, et al., Soft tissue reactions to bioactive glass 13-93 combined with chitosan, J. Biomed. Mater. Res. 83A (2007) 530–537, https://doi.org/10.1002/jbm.a.31225.
[20] R. Guo, X. Hou, D. Zhao, et al., Mechanical stability and biological activity of Mg–Sr co-doped bioactive glass/chitosan composite scaffolds, J. Non-Cryst. Solids 583 (2022) 121481, https://doi.org/10.1016/j.jnoncrysol.2022.121481.
[21] B. Dorj, J.-H. Park, H.-W. Kim, Robocasting chitosan/nanobioactive glass dual-pore structured scaffolds for bone engineering, Mater. Lett. 73 (2012) 119–122, https://doi.org/10.1016/j.matlet.2011.12.107.
[22] M. Bertuola, B. Aráoz, U. Gilabert, et al., Gelatin–alginate–hyaluronic acid inks for 3D printing: effects of bioglass addition on printability, rheology and scaffold tensile modulus, J. Mater. Sci. 56 (2021) 15327–15343, https://doi.org/10.1007/s10853-021-06250-0.
[23] M. Fermani, V. Platania, R.-M. Kavasi, et al., 3D-Printed scaffolds from alginate/methyl cellulose/trimethyl chitosan/silicate glasses for bone tissue engineering, Appl. Sci. 11 (2021) 8677, https://doi.org/10.3390/app11188677.
[24] M.H. Haddadi, E. Karamian, H.R. Bakhsheshi-Rad, M. Kasiri-Asgarani, Investigation of the effect of Bioglass-58S content on structural and biological properties of PCL-chitosan-58S-bioactive glass composite coating for bone tissue engineering application, Ceram. Int. 49 (2023) 8190–8195, https://doi.org/10.1016/j.ceramint.2022.10.343.
[25] W. Xia, J. Chang, Preparation and characterization of nano-bioactive-glasses (NBG) by a quick alkali-mediated sol–gel method, Mater. Lett. 61 (2007) 3251–3253, https://doi.org/10.1016/j.matlet.2006.11.048.
[26] E.M.R. Lee, R. Borges, J. Marchi, et al., Bioactive glass and high-intensity lasers as a promising treatment for dentin hypersensitivity: an in vitro study, J. Biomed. Mater. Res. B Appl. Biomater. 108 (2020) 939–947, https://doi.org/10.1002/jbm.b.34446.
[27] R. Borges, J. Marchi, Sol-gel synthesis of bioglasses: a growth kinetics study by dynamic light scattering, Adv. Sci. Technol. 102 (2017) 18–23. https://doi.org/10.4028/www.scientific.net/AST.102.18.
[28] G.P. Delpino, R. Borges, T. Zambanini, et al., Sol-gel-derived 58S bioactive glass containing holmium aiming brachytherapy applications: a dissolution, bioactivity, and cytotoxicity study, Mater. Sci. Eng. C 119 (2021) 111595, https://doi.org/10.1016/j.msec.2020.111595.
[29] Q. Wu, D. Therriault, M.-C. Heuzey, Processing and properties of chitosan inks for 3D printing of hydrogel microstructures, ACS Biomater. Sci. Eng. 4 (2018) 2643–2652, https://doi.org/10.1021/acsbiomaterials.8b00415.
[30] C.-D. Xue, X.-D. Chen, Y.-J. Li, et al., Breakup dynamics of semi-dilute polymer solutions in a microfluidic flow-focusing device, Micromachines 11 (2020) 406, https://doi.org/10.3390/mi11040406.
[31] Y. Jiang, J. Zhou, C. Feng, et al., Rheological behavior, 3D printability and the formation of scaffolds with cellulose nanocrystals/gelatin hydrogels, J. Mater. Sci. 55 (2020) 15709–15725, https://doi.org/10.1007/s10853-020-05128-x.

[32] Slic3r manual – flow math. https://manual.slic3r.org/advanced/flow-math. (Accessed 31 May 2023).
[33] K.H. Kang, L.A. Hockaday, J.T. Butcher, Quantitative optimization of solid freeform deposition of aqueous hydrogels, Biofabrication 5 (2013) 035001, https://doi.org/10.1088/1758-5082/5/3/035001.
[34] A. Schwab, R. Levato, M. D'Este, et al., Printability and shape fidelity of bioinks in 3D bioprinting, Chem. Rev. 120 (2020) 11028–11055, https://doi.org/10.1021/acs.chemrev.0c00084.
[35] M. Hamdine, M.-C. Heuzey, A. Bégin, Effect of organic and inorganic acids on concentrated chitosan solutions and gels, Int. J. Biol. Macromol. 37 (2005) 134–142, https://doi.org/10.1016/j.ijbiomac.2005.09.009.
[36] G. Gillispie, P. Prim, J. Copus, et al., Assessment methodologies for extrusion-based bioink printability, Biofabrication 12 (2020) 022003, https://doi.org/10.1088/1758-5090/ab6f0d.
[37] J. Nie, Z. Wang, Q. Hu, Chitosan hydrogel structure modulated by metal ions, Nat. Sci. Rep. 6 (2016) 36005, https://doi.org/10.1038/srep36005.
[38] I. Yamaguchi, K. Tokuchi, H. Fukuzaki, et al., Preparation and microstructure analysis of chitosan/hydroxyapatite nanocomposites, J. Biomed. Mater. Res. 55 (2001) 20–27, https://doi.org/10.1002/1097-4636(200104)55:1<20::AID-JBM30>3.0.CO;2-F.
[39] K. Nazemi, F. Moztarzadeh, N. Jalali, et al., Synthesis and characterization of poly (lactic-co-glycolic) acid nanoparticles-loaded chitosan/bioactive glass scaffolds as a localized delivery system in the bone defects, BioMed Res. Int. (2014) 1–9, https://doi.org/10.1155/2014/898930, 2014.
[40] N.S. Kajave, T. Schmitt, T.-U. Nguyen, et al., Bioglass incorporated methacrylated collagen bioactive ink for 3D printing of bone tissue, Biomed. Mater. 16 (2021) 035003, https://doi.org/10.1088/1748-605X/abc744.
[41] M. Sheikhi, F. Rafiemanzelat, S. Ghodsi, et al., 3D printing of jammed self-supporting microgels with alternative mechanism for shape fidelity, crosslinking and conductivity, Addit. Manuf. 58 (2022) 102997, https://doi.org/10.1016/j.addma.2022.102997.
[42] T. Gao, G.J. Gillispie, J.S. Copus, et al., Optimization of gelatin–alginate composite bioink printability using rheological parameters: a systematic approach, Biofabrication 10 (2018) 034106, https://doi.org/10.1088/1758-5090/aacdc7.
[43] A.M. El-Kady, N.A. Kamel, M.M. Elnashar, M.M. Farag, Production of bioactive glass/chitosan scaffolds by freeze-gelation for optimized vancomycin delivery: effectiveness of glass presence on controlling the drug release kinetics, J. Drug Deliv. Sci. Technol. 66 (2021) 102779, https://doi.org/10.1016/j.jddst.2021.102779.
[44] F.E. Ciraldo, E. Boccardi, V. Melli, et al., Tackling bioactive glass excessive in vitro bioreactivity: preconditioning approaches for cell culture tests, Acta Biomater. 75 (2018) 3–10, https://doi.org/10.1016/j.actbio.2018.05.019.
[45] L.M. Marquardt, D. Day, S.E. Sakiyama-Elbert, A.B. Harkins, Effects of borate-based bioactive glass on neuron viability and neurite extension: borate-based Bioactive Glass, J. Biomed. Mater. Res. 102 (2014) 2767–2775, https://doi.org/10.1002/jbm.a.34944.
[46] J.Y. Lim, H.J. Donahue, Cell sensing and response to micro- and nanostructured surfaces produced by chemical and topographic patterning, Tissue Eng. 13 (2007) 1879–1891, https://doi.org/10.1089/ten.2006.0154.
[47] B. Honig, L. Shapiro, Adhesion protein structure, molecular affinities, and principles of cell-cell recognition, Cell 181 (2020) 520–535, https://doi.org/10.1016/j.cell.2020.04.010.